2007 IEEE International Conference on
Robotics and Automation
Roma, Italy, 10-14 April 2007



# Self-Identification of the Joint Centre of a Cable-Driven Shoulder Rehabilitator

Shabbir Kurbanhusen Mustafa[1,2], Guilin Yang[2], Song Huat Yeo[1] and Wei Lin[2]

***Abstract*— This paper presents the joint centre self-identification of a novel cable-driven anthropocentric shoulder rehabilitator. For such a wearable rehabilitator, identification of joint centre is critical for kinematic modeling, path planning and motion control. However, the shoulder joint centre location is unknown when a user wears this rehabilitator and it differs among users. These complicate the initial patient preparatory. A joint centre self-identification model is formulated based on the differential change in the cable end-point distance. A computationally effective algorithm is employed to identify the shoulder joint centre. It does not require any external measurement devices because of the redundant actuation scheme in the cable-driven shoulder rehabilitator. In order to verify the effectiveness and robustness of the proposed algorithm, we conducted computer simulation studies. In the simulation example, although large errors (up to $\pm 50mm$) had been injected into the initial estimates, the joint centre was always accurately identified within four to five iterations.**

## I. INTRODUCTION

In the last decade, the introduction of rehabilitation robots (also known as *Rehabilitators*) has greatly enhanced rehabilitation techniques. These rehabilitators have eased the therapist's load by delivering intensive and repetitive exercise treatments effectively, sometimes achieving dramatically better results than conventional therapy alone [1], [2]. This offers potential hope to millions of patients requiring rehabilitation in their chronic stages. One of the most common limbs requiring rehabilitation is the arm. Hence, greater research efforts have been carried out in this area. Some of the well-known robotic arm rehabilitators used in research include the MIT Manus [1], the ARM Guide [2] and MIME [3]. Inspite of the numerous advantages offered by these arm rehabilitators [1]-[4], they have a common drawback of being designed with a self-deterministic or adjustable self-deterministic structure. This means that the device generates its own characteristic motion that may not coincide with the characteristic motion of the human structure. In addition, most of them are relatively heavy and fixed to a structure or a wall, which limit the user's motion range. Hence these devices cannot fully adapt to the user and place additional stresses on the human joints while carrying out rehabilitation. This may result in greater discomfort and harm to the user.

This work is supported by Nanyang Technological University under Academic Research Fund RG24/06.

[1]School of Mechanical & Aerospace Engineering, Nanyang Technological University, 50 Nanyang Avenue, Singapore 639798 {must0003,myeosh}@ntu.edu.sg

[2]Mechatronics Group, Singapore Institute of Manufacturing Technology, 71 Nanyang Drive, Singapore 638075 {glyang,wlin}@SIMTech.a-star.edu.sg

In order to address the above-mentioned shortcomings, a novel cable-driven anthropocentric arm rehabilitator was proposed in [5] (as shown in Fig. 1). The proposed design combines kinematically under-deterministic cable-driven mechanisms with the human arm structure. The outcome is a deterministic biomechanical structure with improved adaptability and wearability. This 7-DOF arm rehabilitator consists of a 3-DOF shoulder module, a 1-DOF elbow module and a 3-DOF wrist module. Due to the novel design of this 7-DOF cable-driven anthropocentric arm, methods and algorithms developed for existing robotic arms are not readily applicable. Hence, this research was pursued in [6], mainly focusing on issues related to the 3-DOF shoulder module. This is because the wrist module analysis is similar to that of the 3-DOF shoulder module, while the 1-DOF elbow module analysis is a trivial case. Thus, once the shoulder module analysis is completed, the analysis of the whole 7-DOF arm can also be readily conducted.

For such a wearable shoulder rehabilitator, one of the critical issues to address is the identification of the shoulder joint centre location which is crucial for kinematic modeling and motion control. An inaccurate kinematic model will in turn affect the positioning accuracy and the performance capabilities of the shoulder rehabilitator. This joint centre location with respect to the rehabilitator base is unknown and cannot be determined directly from physical measurements. Furthermore, it varies with each user. These complicate the initial patient preparatory and subsequent utilization of the shoulder rehabilitator.

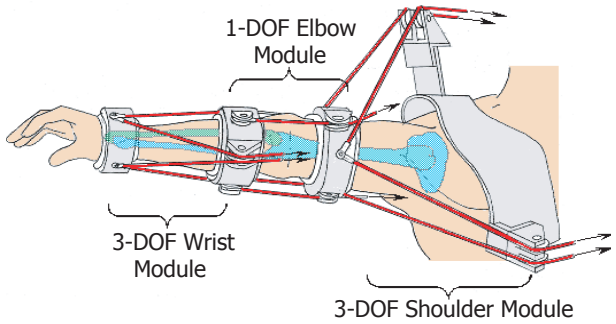


Fig. 1. Conceptual design of the cable-driven anthropocentric arm rehabilitator [5]

The shoulder joint is usually modeled as a perfect 'ball-&-socket' with a fixed centre of rotation located at the geometric centre of the humeral head [7]. The earliest method used to estimate the shoulder joint centre was skin-based. This location was approximated as '*two inches inferior of the right acromion on the lateral surface of the upper arm*'

[8]. Shoulder joint centre identification has since advanced from skin-based estimation methods to vision and optical based methods [9,10]. However, these advanced methods require costly motion tracking cameras to capture the data and complex data acquisition systems to process the captured data. Hence there is a need to come up with a relatively accurate yet cost effective method to determine the shoulder joint centre for the users of this shoulder rehabilitator.

The design optimization of the shoulder rehabilitator was carried out in [6], in which the optimized design was a 3-3 six-cable configuration, as shown in Fig. 2. This 3-DOF shoulder rehabilitator has a redundant actuation scheme, driven by six redundant cables. By observation of this 3-3 configuration, the cable end-points $P_i$ $(i = 1,2,3)$ of the optimized configuration formed the vertex of three tetrahedrons (shown in Fig. 3). Thus, by utilizing the 'Tetrahedron' proposition [11] and the six cable length data, we can determine the distance between the cable end-points i.e. $p_{12}$, $p_{23}$ and $p_{31}$. The cable end-point distance measurement residues (i.e. the difference between the computed and the actual values of $p_{12}$, $p_{23}$ and $p_{31}$) will then allow us to formulate a self-identification model to determine the actual joint centre location for any users of the shoulder rehabilitator. This model is termed as *self-identification* because it does not require any additional external measurement devices. Instead, the available motor encoders will provide the cable length information needed to carry out the joint centre self-identification.

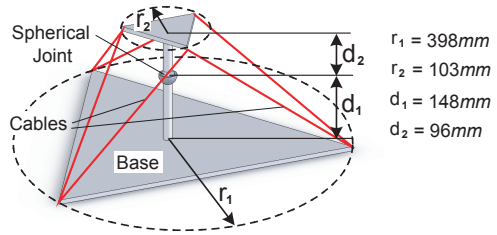


Fig. 2. Optimized design of the shoulder rehabilitator: 3-3 six-cable configuration [6]

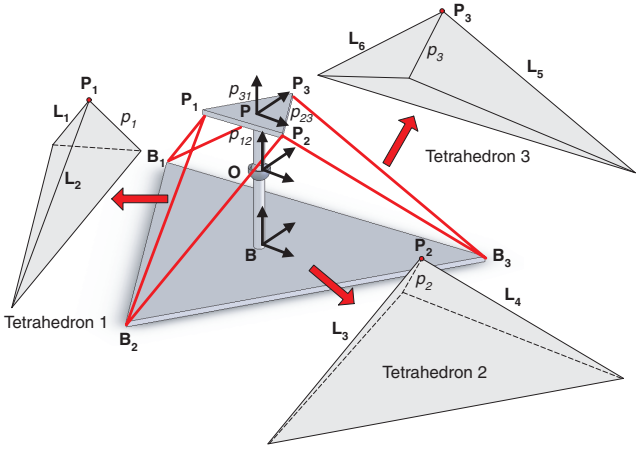


Fig. 3. Kinematic model of the shoulder rehabilitator with observed tetrahedrons

In terms of the initial patient preparatory, after wearing the shoulder rehabilitator, the user simply needs to position it at a number of poses and obtain the readily available cable length data measurements. The initial estimate for the joint centre will be the skin-based location [8] mentioned previously. The proposed algorithm will then use these data and the known mechanism parameters to determine the actual shoulder joint centre location. The next section will present the joint centre self-identification methodology, including the kinematic modeling of the shoulder rehabilitator and the joint centre self-identification algorithm. This will be followed by computer simulation examples to validate the accuracy and robustness of the proposed joint centre self-identification model.

## II. JOINT CENTRE SELF-IDENTIFICATION METHODOLOGY

This section will present the joint centre self-identification model followed by the self-identification algorithm. Similar to robotic manipulator calibration [12], the joint centre self-identification process consists of three main steps: modeling, measurement and identification. The 'Modeling' step refers to the formulation of a suitable joint centre identification model which will relate the cable end-point distance measurement residues to the joint centre parameters to be identified, based on the measurement data of the six cable lengths. This is followed by the 'Measurement' step which refers to the collection of the six cable lengths which can be obtained from the motor encoders used in the actual shoulder rehabilitator. Lastly, the 'Identification' step is to determine the actual joint centre location of the shoulder rehabilitator based on the joint centre self-identification model and the measurement data.

### A. Joint Centre Self-Identification Model

Before proceeding to the description of the self-identification model, the kinematic model of the cable-driven shoulder rehabilitator is first described in order to provide a better understanding of this model development. Three coordinate frames (i.e. $\{\mathrm{B}\}$, $\{\mathrm{O}\}$ and $\{\mathrm{P}\}$) are used to describe its kinematic model (as shown in Fig. 3). Frame $\{\mathrm{B}\}$ is the inertial coordinate frame on the base platform. Frame $\{\mathrm{O}\}$ is located at the shoulder joint centre, which undergoes only a translation $\overrightarrow{BO} = \{x,y,z\}^T$ wrt $\{\mathrm{B}\}$. Frame $\{\mathrm{P}\}$ is the local coordinate frame on the moving platform which undergoes a translation $\overrightarrow{OP}$ and a rotation $R_{OP}$ wrt $\{\mathrm{O}\}$. $\overrightarrow{BB_i}$s are base cable attachment point position vectors that are fixed with respect to $\{\mathrm{B}\}$, while $\overrightarrow{PP_i}$s are cable end-point position vectors that are fixed with respect to $\{\mathrm{P}\}$.

The objective of the self-identification model is to identify the unknown joint centre location through observations of the measurement residues in certain parameters of the mechanism. The first step in formulating this model is to identify the relevant parameters and to obtain the relationship equations between them. At any feasible pose, the known measurable parameters are the set of six cable lengths, the position vectors of the cable attachment points, $\overrightarrow{BB_i}$ and $\overrightarrow{PP_i}$ $(i = 1,2,3)$, and the lengths of $p_{12}$, $p_{23}$ and $p_{31}$. The unknown parameters are $\overrightarrow{BO}$ and $\overrightarrow{OP_i}$ $(i = 1,2,3)$ since we do not know the actual location of the shoulder joint centre.

Hence, these values have to be estimated in the kinematic model (Note: The mechanism is assumed to have error-free fabrication and assembly in order to simplify the model). At each point $P_i$, several distance relationship equations can be obtained.

The distance relationship equations at point $P_1$ are as follows:

$$p_1 = \left\| \overrightarrow{OP_1} \right\| \tag{1}$$

$$L_1 = \left\| \overrightarrow{B_1B} + \overrightarrow{BO} + \overrightarrow{OP_1} \right\| \tag{2}$$

$$L_2 = \left\| \overrightarrow{B_2B} + \overrightarrow{BO} + \overrightarrow{OP_1} \right\| \tag{3}$$

The distance relationship equations at point $P_2$ are as follows:

$$p_2 = \left\| \overrightarrow{OP_2} \right\| \tag{4}$$

$$L_3 = \left\| \overrightarrow{B_2B} + \overrightarrow{BO} + \overrightarrow{OP_2} \right\| \tag{5}$$

$$L_4 = \left\| \overrightarrow{B_3B} + \overrightarrow{BO} + \overrightarrow{OP_2} \right\| \tag{6}$$

The distance relationship equations at point $P_3$ are as follows:

$$p_3 = \left\| \overrightarrow{OP_3} \right\| \tag{7}$$

$$L_5 = \left\| \overrightarrow{B_3B} + \overrightarrow{BO} + \overrightarrow{OP_3} \right\| \tag{8}$$

$$L_6 = \left\| \overrightarrow{B_1B} + \overrightarrow{BO} + \overrightarrow{OP_3} \right\| \tag{9}$$

In addition, due to the unique 3-3 configuration of the shoulder rehabilitator (shown in Fig. 3), the 'Tetrahedron' approach [11] can be utilized to obtain the position vectors $\overrightarrow{OP_i}$ $(i = 1,2,3)$. Based on the 'Tetrahedron' proposition, the top vertex (i.e. $P_i$) can be uniquely determined with respect to a tetrahedron coordinate (i.e. Base Frame $\{\mathrm{B}\}$) provided two known base vectors (i.e. base cable attachment point vectors with respect to $\{\mathrm{O}\}$) and three known space lines (i.e. the lengths of the two cables attached to $P_i$ and the length of $\overrightarrow{OP_i}$) are known. This will determine the cable end-point distances $p_{12}$, $p_{23}$ and $p_{31}$. The presence of errors in the estimates of the joint centre location can then be identified by comparing the differences in the computed and actual values of $p_{12}$, $p_{23}$ and $p_{31}$. If there is no difference, this means that the estimation of the joint centre location is accurate. The following relationship equations are obtained for $p_{12}$, $p_{23}$ and $p_{31}$:

$$p_{12} = \left\| \overrightarrow{P_1P_2} \right\| = \left\| \overrightarrow{OP_1} - \overrightarrow{OP_2} \right\| \tag{10}$$

$$p_{23} = \left\| \overrightarrow{P_2P_3} \right\| = \left\| \overrightarrow{OP_2} - \overrightarrow{OP_3} \right\| \tag{11}$$

$$p_{31} = \left\| \overrightarrow{P_3P_1} \right\| = \left\| \overrightarrow{OP_3} - \overrightarrow{OP_1} \right\| \tag{12}$$

The next step is to obtain the differential relationship between $x$, $y$, $z$, $p_1$, $p_2$ and $p_3$ (these contribute to the kinematic errors), and $p_{12}$, $p_{23}$ and $p_{31}$ (these evaluate the presence of the kinematic errors). Hence Eq. (1)-(12) are differentiated and the resulting linear differential equations are rearranged to obtain the joint centre self-identification model (Refer to Appendix for details). This model will allow identification of the joint centre location through observations of the cable end-point distance measurement residues. At any pose, the joint centre self-identification model is described as:

$$Y = D \cdot X \tag{13}$$

Where $Y = \{\delta p_{12}, \delta p_{23}, \delta p_{31}\}^T \in \Re^{3\times 1}$, $D \in \Re^{3\times 6}$ and $X = \{\delta x, \delta y, \delta z, \delta p_1, \delta p_2, \delta p_3\}^T \in \Re^{6\times 1}$. For the terms in $Y$, $\delta p = p^{actual} - p^{computed}$. $p^{actual}$ is determined from the actual measurements made on the mechanism structure, while $p^{computed}$ is determined from Eq. (10)-(12) using $\overrightarrow{OP_i}$. On the other hand, $\overrightarrow{OP_i}$ is determined using the tetrahedron approach which requires the actual cable length data $(L_1, \ldots, L_6)$ and estimated values of $p_i$ $(i = 1,2,3)$. $D$ is the joint centre self-identification Jacobian matrix which consists of linear terms that are functions of $\overrightarrow{BB_i}$, $\overrightarrow{OP_i}$, $x$, $y$, $z$, $p_1$, $p_2$, $p_3$, $p_{12}$, $p_{23}$ and $p_{31}$. It describes the gross errors in $p_{12}$, $p_{23}$ and $p_{31}$ resulting from the errors in the estimates of $x$, $y$, $z$, $p_1$, $p_2$ and $p_3$. Based on Eq. (13), as the initial estimates of $x$, $y$, $z$, $p_1$, $p_2$ and $p_3$ approach the actual values of the mechanism, the term $Y$ will also approach zero.

### *B. Joint Centre Self-Identification Algorithm*

Similar to the iterative calibration procedure in [13], a least-squares algorithm based on the proposed self-identification model in Eq. (13) is employed to determine the joint centre solution. In order to obtain reliable results for the joint centre location, it is required to take measurements at several poses. For $m$ sets of measurement poses, the $i^{th}$ pose with its set of cable length data measurements will result in $Y_i$ and its corresponding $D_i$. After $m$ sets of measurement data, $Y_i$ and $D_i$ are stacked to form the following equation:

$$\widetilde{Y} = \widetilde{D} \cdot X \tag{14}$$

Where $\widetilde{Y} = \{Y_1, \ldots, Y_m\}^T \in \Re^{3m\times 1}$ and $\widetilde{D} = \{D_1, \ldots, D_m\}^T \in \Re^{3m\times 6}$. Since the model in Eq. (14) contains $3m$ linear equations with 6 variables, the least-squares algorithm is used (Note: Eq. (14) must have at least two measurement poses). The least-squares solution of $X$ is given as:

$$X = (\widetilde{D}^T \widetilde{D})^{-1} \cdot \widetilde{D}^T \cdot Y \tag{15}$$

Where $(\widetilde{D}^T \widetilde{D})^{-1} \widetilde{D}^T$ is the pseudo-inverse of $\widetilde{D}$. The solution of Eq. (15) is further improved through iterative substitution as shown in Fig. 4. A refinement in the least-squares algorithm can be achieved by iterative looping. Once the kinematic error parameter vector, $X$ is identified, estimates of $x$, $y$, $z$, $p_1$, $p_2$ and $p_3$ are updated after every loop $i$ by substituting $X$ into the following equation:

$$\begin{Bmatrix} x \\ y \\ z \\ p_1 \\ p_2 \\ p_3 \end{Bmatrix}_{i+1} = X + \begin{Bmatrix} x \\ y \\ z \\ p_1 \\ p_2 \\ p_3 \end{Bmatrix}_{i} \tag{16}$$

This procedure is repeated until the deviation metric, $\delta E$ approaches a certain tolerance limit, $\varepsilon$, which is close to

zero. Then the final $x$, $y$, $z$, $p_1$, $p_2$ and $p_3$ will represent the actual parameters of the bio-kinematic shoulder rehabilitator structure. $\delta E$ is the average measurement residue of $p_{12}$, $p_{23}$ and $p_{31}$, and is mathematically defined as:

$$\delta E = \sqrt{\frac{1}{3m}(Y^T \cdot Y)} \tag{17}$$

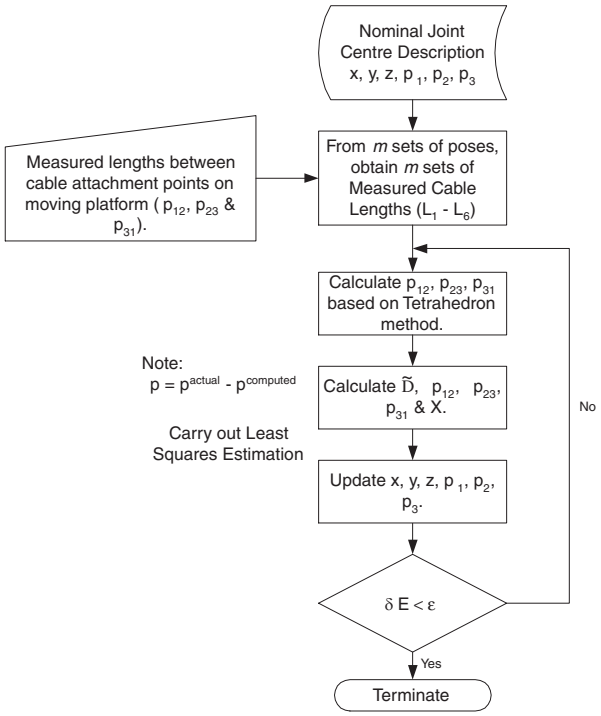


Fig. 4. Iterative Joint Centre Self-Identification Algorithm Flowchart

## III. COMPUTER SIMULATION

In this section, simulation studies were carried out on the optimized 3-3 six-cable shoulder rehabilitator shown in Fig. 2. In the real situation, the actual joint centre location is unknown. However, in order to evaluate the joint centre self-identification algorithm, the actual location is assumed to be known and the initial estimated location will be varied. Initial estimates with deviations about the actual joint centre location will be used to test the accuracy and robustness of the joint centre self-identification algorithm. The first simulation will investigate the effects of the initial estimates of $x$, $y$, $z$, $p_1$, $p_2$ and $p_3$ under ideal experimental conditions (i.e. noise-free cable length data measurements). The second simulation will investigate the effect of noise in cable length data measurements. For the simulation studies, the following procedure is employed:

1) Generate two sets of $m$ random poses (within the limits of the shoulder joint motion range) and their corresponding 'simulated' cable length data. This is based on Eqs. (2), (3), (5), (6), (8) and (9), and the actual kinematic parameters listed in Table I. The first set will be used for joint centre identification, while the second set will be used for verification.

TABLE I
ACTUAL KINEMATIC PARAMETERS OF THE SHOULDER REHABILITATOR

| Parameter Description† | Actual Value‡ ($mm$) |
|---|---|
| $\overrightarrow{BO}^{\{B\}} = \{x,y,z\}^T$ | $\{0,0,148\}^T$ |
| $\overrightarrow{OP}^{\{P\}} = \{0,0,d_2\}^T$ | $\{0,0,96\}^T$ |
| $p_1 = \|\overrightarrow{OP} + \overrightarrow{PP_1}\|$ | 140.8 |
| $p_2 = \|\overrightarrow{OP} + \overrightarrow{PP_2}\|$ | 140.8 |
| $p_3 = \|\overrightarrow{OP} + \overrightarrow{PP_3}\|$ | 140.8 |
| $p_{12} = \|\overrightarrow{PP_1} - \overrightarrow{PP_2}\|$ | 178.4 |
| $p_{23} = \|\overrightarrow{PP_2} - \overrightarrow{PP_3}\|$ | 178.4 |
| $p_{31} = \|\overrightarrow{PP_3} - \overrightarrow{PP_1}\|$ | 178.4 |

†The letter in the superscript refers to the coordinate frame which the vectors are based upon.
‡These values are based on the 'home' position of the shoulder rehabilitator. 'Home' is the pose where all six cables have equal lengths as shown in Fig. 2 and $R_{OP}$ is an Identity matrix.

2) Assign errors in the actual values of the kinematic parameters $x$, $y$, $z$, $p_1$, $p_2$ and $p_3$ (listed in Table I), to be used as initial estimates.
3) Identify the actual shoulder joint centre location using the joint centre self-identification algorithm and the first set of $m$ 'simulated' cable length data.
4) Verify the identified joint centre using the second set of $m$ 'simulated' cable length data.

### A. Effect of Initial Parameter Estimate

In this simulation study, it is assumed that the set of cable length measurement at each pose are noise-free (i.e. ideal measurements). The theoretical lower bound for the number of measured poses is two but for accuracy and robustness, it is set to three. From the viewpoint of computer simulation, the initial estimate errors $\{\delta x, \delta y, \delta z\}$ and $\{\delta p_1, \delta p_2, \delta p_3\}$ are randomly generated with uniformly distributed deviations of $\pm d$.

From the simulation results in Table II, assigned errors with uniformly distributed deviations of up to $\pm 50mm$ are fully recovered within 4 to 5 iterations. This demonstrates the accuracy of the joint centre self-identification model for the wearable shoulder rehabilitator. Fig. 5 shows the joint centre identification convergence plot for errors in initial estimates with uniformly distributed deviations of $\pm 50mm$. $\delta E$ is driven from an initial value of 31.57 to approximately zero within 4 iterations.

### B. Effect of Noise in Cable Length Data Measurement

In practical applications, it is impossible to have noise-free measurements. Hence this simulation study will investigate the robustness of the joint centre self-identification model by introducing noise in the cable length measurement. From the viewpoint of computer simulation, a randomly generated noise $\delta L_i$ $(i = 1, \ldots, 6)$ with uniformly distributed deviation of $\pm \ell$ will be injected into the 'simulated' cable length measurement. In addition, more measurement poses will also be considered since noise exists. In each simulation, two sets of 100 simulated measurement poses are used. One set is

TABLE II

SIMULATION RESULTS ON EFFECTS OF INITIAL PARAMETER ESTIMATE

| d | Assigned Error in Actual Parameters $\{\delta x, \delta y, \delta z, \delta p_1, \delta p_2, \delta p_3\}$ | Error after Self-Identification $\{\delta x, \delta y, \delta z, \delta p_1, \delta p_2, \delta p_3\}$ |
|---|---|---|
| 10 | $\{2.54, -1.39, 8.36,$ $9.56, -4.21, 5.23\}$ | $\{-8.12, 4.35, -1.76,$ $1.26, -6.79, 1.33\} \times 10^{-9}$ |
| 30 | $\{18.44, 25.37, 14.61,$ $-8.05, -28.8, 25.44\}$ | $\{-6.92, 1.31, -5.04,$ $4.28, 7.23, 1.08\} \times 10^{-7}$ |
| 50 | $\{-45.02, -17.8, -45.55,$ $7.95, -45.29, -40.33\}$ | $\{7.34, 6.31, -1.84,$ $-1.06, 9.3, 4.96\} \times 10^{-6}$ |

All dimensions are in millimeters. $\varepsilon$ is set to $1 \times 10^{-3}$.

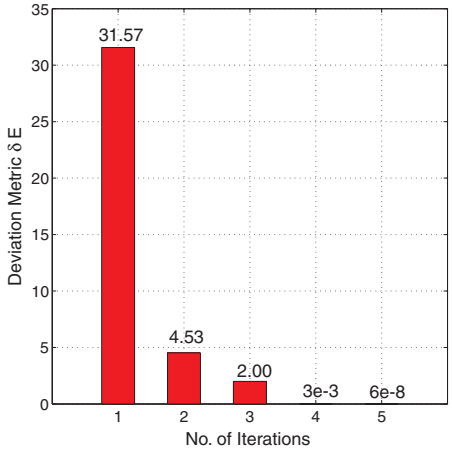


Fig. 5. Joint Center Self-Identification Convergence Plot with noise-free measurements ($d$ = 50$mm$)

used to identify the joint centre, while the other set is used to verify the result of the joint centre self-identification.

With the existence of measurement noise, full recovery of the assigned errors cannot be achieved. However, from Fig. 6 and 7, it is observed in both cases that the deviation metric $\delta E$ converges to about 0.07$mm$ (with $\ell = 0.1mm$) when the number of measurement poses is greater than 30. This implies that the assigned errors in the actual joint centre parameters are precisely identified.

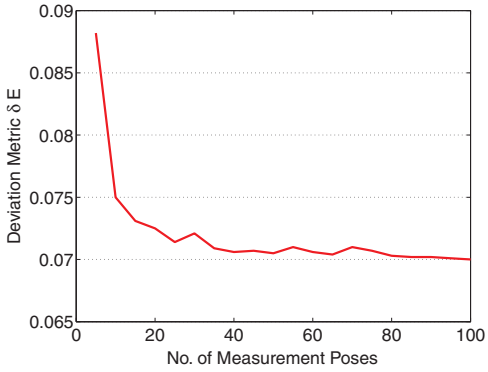


Fig. 6. Quantified deviation metric plot versus number of measurement poses with $d$ = 25$mm$ and $\ell$ = 0.1$mm$

## IV. CONCLUSION

The joint centre self-identification is to locate the actual shoulder joint centre of the shoulder rehabilitator user without the use of any external measurement devices. Instead, it is based on the redundant actuation scheme of the cable-driven shoulder rehabilitator and the available motor encoder readings. A joint centre self-identification model is developed based on the cable end-point distance measurement residue. This model has a linear form and an iterative least-squares approach is used to identify the actual joint centre from an initial estimate.

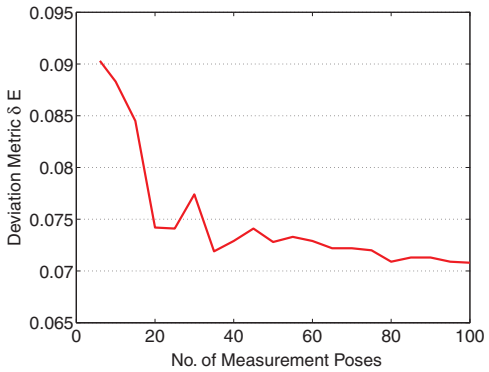


Fig. 7. Quantified deviation metric plot versus number of measurement poses with $d$ = 50mm and $\ell$ = 0.1$mm$

Simulation studies on the shoulder rehabilitator demonstrate that the joint centre can be fully recovered with assigned errors of up to $\pm 50mm$, under noise-free measurement conditions. In the presence of measurement noise, the assigned errors can also be precisely recovered with a certain number of minimum measurement poses. Hence this self-identification model is able to accurately and robustly identify the shoulder joint centre location of a user wearing the shoulder rehabilitator. Future works will focus on the experimental study of the proposed joint centre self-identification algorithm on a shoulder rehabilitator prototype.

## V. ACKNOWLEDGMENT

Mustafa S.K. would like to thank the Agency for Science, Technology & Research for awarding the PhD scholarship. The authors would also like to thank Prof I-Ming Chen from the School of MAE, NTU.

## REFERENCES

[1] H. I. Krebs, N. Hogan, M. L. Aisen, and B. T. Volpe, "Robot-Aided Neurorehabilitation", *IEEE Transactions on Rehabilitation Engineering*, vol. 6, no. 1, pp. 75-87, 1998.

[2] D. J. Reinkensmeyer, L. E. Kahn, M. Averbuch, A. McKenna-Cole, B. D. Schmit, and W. Z. Rymer, "Understanding and Treating Arm Movement Impairment after Chronic brain Injury: Progress with the ARM Guide", *Journal of Rehabilitation Research and Development*, vol. 37, 2000.

[3] P. S. Lum, C. G. Burgar, D. E. Kenney, and H. F. M. Van der Loos, "Quantification of force abnormalities during passive and active-assisted upper-limb reaching movements in post-stroke hemiparesis", *IEEE Transactions on Biomedical Engineering*, vol. 46, pp. 652-662, 1999.

[4] N. G. Tsagarakis and D. G. Caldwell, "Development and Control of a 'Soft-Actuated' Exoskeleton for Use in Physiotherapy and Training", *Autonomous Robots*, vol. 15, pp. 21-33, 2003.

[5] G. Yang, H. L. Ho, W. Chen, W. Lin, and M. S. Kurbanhusen, "A Haptic Device Wearable on a Human Arm", *in Proc. of IEEE Conference on Robotics, Automation And Mechatronics*, pp. 243-248, Singapore, 2004.

[6] S.K. Mustafa, G. Yang, S.H. Yeo, and W. Lin, "Optimal Design of a Bio-Inspired Anthropocentric Shoulder Rehabilitator", *Journal of Applied Bionics and Biomechanics*, vol. 3, no. 3, pp. 199-208, 2006.

[7] H.E.J. Veeger, "The Position Of The Rotation Center Of The Gleno-humeral Joint", *Journal of Biomechanics*, vol. 33, pp. 1711-1715, 2000.

[8] CGA FAQ: Joint Centre Estimation [Internet], Available: http://www.univie.ac.at/cga/faq/centre.html, Last visited: 02\01\07.

[9] L. Mundermann, S. Corazza, and T.P. Andriacchi, "The evolution of methods for the capture of human movement leading to markerless motion capture for biomechanical applications", *Journal of Neuro-engineering Rehabilitation*, vol. 3, issue 6, 2006.

[10] G. Rau, C. Disselhorst-Klug, and R. Schmidt, "Movement Biomechanics goes upwards: from the leg to the arm", *Journal Of Biomechanics*, vol. 33, pp. 1207-1216, 2000.

[11] S.-K. Song and D.-S. Kwon, "Efficient formulation approach for the forward kinematics of the 3-6 Stewart-Gough Platform", *in Proc. of IEEE/RSJ International Conference on Intelligent Robots and Systems*, 2001.

[12] B.W. Mooring, Z.S. Roth, and M.R. Driels, *Fundamentals of manipulator calibration*, New York: John Wiley & Sons, 1991.

[13] G. Yang, I.-M. Chen, W.K. Lim, and S.H. Yeo, "Self-calibration of three-legged modular reconfigurable parallel robots based on leg-end distance errors", *Robotica*, vol. 19, pp. 187-198, 2001.


## APPENDIX

Using mathematical tools from differential theory, the following differential equations are obtained for Eq. (1)-(12):
(Note that $\overrightarrow{OP_i} = \{p_{xi}, p_{yi}, p_{zi}\}^T$ and $\overrightarrow{BB_i} = \{b_{xi}, b_{yi}, b_{zi}\}^T$)

$$Eq.(1) \Rightarrow p_1 \delta p_1 = \{p_{x1}, p_{y1}, p_{z1}\} \cdot \{\delta p_{x1}, \delta p_{y1}, \delta p_{z1}\}^T \tag{A1}$$

$$Eq.(2) \Rightarrow \begin{Bmatrix} (b_{x1}-x-p_{x1}) \\ (b_{y1}-y-p_{y1}) \\ (b_{z1}-z-p_{z1}) \end{Bmatrix}^T . \begin{Bmatrix} \delta x \\ \delta y \\ \delta z \end{Bmatrix} = \begin{Bmatrix} (x-b_{x1}+p_{x1}) \\ (y-b_{y1}+p_{y1}) \\ (z-b_{z1}+p_{z1}) \end{Bmatrix}^T . \begin{Bmatrix} \delta p_{x1} \\ \delta p_{y1} \\ \delta p_{z1} \end{Bmatrix} \tag{A2}$$

$$Eq.(3) \Rightarrow \begin{Bmatrix} (b_{x2}-x-p_{x1}) \\ (b_{y2}-y-p_{y1}) \\ (b_{z2}-z-p_{z1}) \end{Bmatrix}^T . \begin{Bmatrix} \delta x \\ \delta y \\ \delta z \end{Bmatrix} = \begin{Bmatrix} (x-b_{x2}+p_{x1}) \\ (y-b_{y2}+p_{y1}) \\ (z-b_{z2}+p_{z1}) \end{Bmatrix}^T . \begin{Bmatrix} \delta p_{x1} \\ \delta p_{y1} \\ \delta p_{z1} \end{Bmatrix} \tag{A3}$$

From $Eq.(A1)-(A3)$, we obtain:

$$\begin{Bmatrix} \delta p_{x1} \\ \delta p_{y1} \\ \delta p_{z1} \end{Bmatrix} = {A_1}^{-1}.B_1.\begin{Bmatrix} \delta x \\ \delta y \\ \delta z \\ \delta p_1 \end{Bmatrix} \tag{A4}$$

Where:

$$A_1 = \begin{bmatrix} (x-b_{x1}+p_{x1}) & (y-b_{y1}+p_{y1}) & (z-b_{z1}+p_{z1}) \\ (x-b_{x2}+p_{x1}) & (y-b_{y2}+p_{y1}) & (z-b_{z2}+p_{z1}) \\ p_{x1} & p_{y1} & p_{z1} \end{bmatrix}$$

$$B_1 = \begin{bmatrix} (b_{x1}-x-p_{x1}) & (b_{y1}-y-p_{y1}) & (b_{z1}-z-p_{z1}) & 0 \\ (b_{x2}-x-p_{x1}) & (b_{y2}-y-p_{y1}) & (b_{z2}-z-p_{z1}) & 0 \\ 0 & 0 & 0 & p_1 \end{bmatrix}$$

Similarly, from the differential equations of $Eq.(4)-(9)$, we obtain:

$$\begin{Bmatrix} \delta p_{x2} \\ \delta p_{y2} \\ \delta p_{z2} \end{Bmatrix} = {A_2}^{-1}.B_2.\begin{Bmatrix} \delta x \\ \delta y \\ \delta z \\ \delta p_2 \end{Bmatrix} \tag{A5}$$

And,

$$\begin{Bmatrix} \delta p_{x3} \\ \delta p_{y3} \\ \delta p_{z3} \end{Bmatrix} = {A_3}^{-1}.B_3.\begin{Bmatrix} \delta x \\ \delta y \\ \delta z \\ \delta p_3 \end{Bmatrix} \tag{A6}$$

Where:

$$A_2 = \begin{bmatrix} (x-b_{x2}+p_{x2}) & (y-b_{y2}+p_{y2}) & (z-b_{z2}+p_{z2}) \\ (x-b_{x3}+p_{x2}) & (y-b_{y3}+p_{y2}) & (z-b_{z3}+p_{z2}) \\ p_{x2} & p_{y2} & p_{z2} \end{bmatrix}$$

$$B_2 = \begin{bmatrix} (b_{x2}-x-p_{x2}) & (b_{y2}-y-p_{y2}) & (b_{z2}-z-p_{z2}) & 0 \\ (b_{x3}-x-p_{x2}) & (b_{y3}-y-p_{y2}) & (b_{z3}-z-p_{z2}) & 0 \\ 0 & 0 & 0 & p_2 \end{bmatrix}$$

$$A_3 = \begin{bmatrix} (x-b_{x3}+p_{x3}) & (y-b_{y3}+p_{y3}) & (z-b_{z3}+p_{z3}) \\ (x-b_{x1}+p_{x3}) & (y-b_{y1}+p_{y3}) & (z-b_{z1}+p_{z3}) \\ p_{x3} & p_{y3} & p_{z3} \end{bmatrix}$$

$$B_3 = \begin{bmatrix} (b_{x3}-x-p_{x3}) & (b_{y3}-y-p_{y3}) & (b_{z3}-z-p_{z3}) & 0 \\ (b_{x1}-x-p_{x3}) & (b_{y1}-y-p_{y3}) & (b_{z1}-z-p_{z3}) & 0 \\ 0 & 0 & 0 & p_3 \end{bmatrix}$$

$$Eq.(10) \Rightarrow p_{12}\delta p_{12} = \underbrace{\begin{Bmatrix} p_{x1}-p_{x2} \\ p_{y1}-p_{y2} \\ p_{z1}-p_{z2} \end{Bmatrix}^T}_{Matrix\,C_1} . \begin{Bmatrix} \delta p_{x1}-\delta p_{x2} \\ \delta p_{y1}-\delta p_{y2} \\ \delta p_{z1}-\delta p_{z2} \end{Bmatrix} \tag{A7}$$

$$Eq.(11) \Rightarrow p_{23}\delta p_{23} = \underbrace{\begin{Bmatrix} p_{x2}-p_{x3} \\ p_{y2}-p_{y3} \\ p_{z2}-p_{z3} \end{Bmatrix}^T}_{Matrix\,C_2} . \begin{Bmatrix} \delta p_{x2}-\delta p_{x3} \\ \delta p_{y2}-\delta p_{y3} \\ \delta p_{z2}-\delta p_{z3} \end{Bmatrix} \tag{A8}$$

$$Eq.(12) \Rightarrow p_{31}\delta p_{31} = \underbrace{\begin{Bmatrix} p_{x3}-p_{x1} \\ p_{y3}-p_{y1} \\ p_{z3}-p_{z1} \end{Bmatrix}^T}_{Matrix\,C_3} . \begin{Bmatrix} \delta p_{x3}-\delta p_{x1} \\ \delta p_{y3}-\delta p_{y1} \\ \delta p_{z3}-\delta p_{z1} \end{Bmatrix} \tag{A9}$$

Substituting $(A4)$ and $(A5)$ into $Eq.(A7)$, we obtain:

$$\delta p_{12} = \underbrace{\frac{1}{p_{12}} C_1 {A_1}^{-1} B_1}_{Matrix\,D_{11}} \begin{Bmatrix} \delta x \\ \delta y \\ \delta z \\ \delta p_1 \end{Bmatrix} - \underbrace{\frac{1}{p_{12}} C_1 {A_2}^{-1} B_2}_{Matrix\,D_{12}} \begin{Bmatrix} \delta x \\ \delta y \\ \delta z \\ \delta p_2 \end{Bmatrix} \tag{A10}$$

Substituting $(A5)$ and $(A6)$ into $Eq.(A8)$, we obtain:

$$\delta p_{23} = \underbrace{\frac{1}{p_{23}} C_2 {A_2}^{-1} B_2}_{Matrix\,D_{21}} \begin{Bmatrix} \delta x \\ \delta y \\ \delta z \\ \delta p_2 \end{Bmatrix} - \underbrace{\frac{1}{p_{23}} C_2 {A_3}^{-1} B_3}_{Matrix\,D_{22}} \begin{Bmatrix} \delta x \\ \delta y \\ \delta z \\ \delta p_3 \end{Bmatrix} \tag{A11}$$

Substituting $(A6)$ and $(A4)$ into $Eq.(A9)$, we obtain:

$$\delta p_{31} = \underbrace{\frac{1}{p_{31}} C_3 {A_3}^{-1} B_3}_{Matrix\,D_{31}} \begin{Bmatrix} \delta x \\ \delta y \\ \delta z \\ \delta p_3 \end{Bmatrix} - \underbrace{\frac{1}{p_{31}} C_3 {A_1}^{-1} B_1}_{Matrix\,D_{32}} \begin{Bmatrix} \delta x \\ \delta y \\ \delta z \\ \delta p_1 \end{Bmatrix} \tag{A12}$$

Combining $Eq.(A10), (A11)$ and $(A12)$, we obtain the joint centre self-identification model (i.e. $Eq.(13)$) as follows:

$$Y = D \cdot X \tag{A13}$$

Where:

$$Y = \begin{Bmatrix} \delta p_{12} \\ \delta p_{23} \\ \delta p_{31} \end{Bmatrix},$$

$$D = \begin{bmatrix} (D_{11(1)}-D_{12(1)}) & (D_{21(1)}-D_{22(1)}) & (D_{31(1)}-D_{32(1)}) \\ (D_{11(2)}-D_{12(2)}) & (D_{21(2)}-D_{22(2)}) & (D_{31(2)}-D_{32(2)}) \\ (D_{11(3)}-D_{12(3)}) & (D_{21(3)}-D_{22(3)}) & (D_{31(3)}-D_{32(3)}) \\ D_{11(4)} & 0 & -D_{32(4)} \\ -D_{12(4)} & D_{21(4)} & 0 \\ 0 & -D_{22(4)} & D_{31(4)} \end{bmatrix}^T,$$

And $X = \{ \ \delta x \quad \delta y \quad \delta z \quad \delta p_1 \quad \delta p_2 \quad \delta p_3 \ \}^T$.